IEEE Access
Multidisciplinary | Rapid Review | Open Access Journal

Received August 26, 2019, accepted September 12, 2019, date of publication October 2, 2019, date of current version October 17, 2019.

Digital Object Identifier 10.1109/ACCESS.2019.2945036

Novel Low Noise Amplifier for Neural Signals Based on STT-MTJ Spintronic Device

GUANGCHEN PAN, ALI KARYMY, PINGPING YU, AND YANFENG JIANG, (Senior Member, IEEE)
Department of Microelectronics, Internet of Things Engineering College, Jiangnan University, Wuxi 214122, China

Corresponding author: Yanfeng Jiang (jiangyf@jiangnan.edu.cn)

This work was supported in part by the National Natural Science Foundation of China under Grant 61774078 and Grant 51802124, in part by the Natural Science Foundation of Jiangsu Province under Grant BK 20180626, and in part by the Fundamental Research Funds for the Central Universities under Grant JUSRP11858.

ABSTRACT Low noise amplifier is generally adopted in brain-machine interface (BMI) for the purpose of the extraction of action potentials of neural signals from the Local Field Potentials (LFPs). However, the frequency ranges of these signals are very near to those of the LFPs and other existing noises. So the matter brings us difficulties in order to designing of the amplifier. The purpose of this paper is concentrated on designing of a low noise amplifier specific for the neural signals. Based on the STT-MTJ spintronic devices, the amplifier selectively amplifies the high amplitude peaks, while suppresses the low amplitude peaks. In this way, the novel amplifier can be used to amplify the useful neural signals not only based on the frequency but also on the amplitude. At the same time, the noise signals are suppressed by the amplifier. The low cut-off frequency of the amplifier is adjusted to be 1.24 Hz. The gain of the amplifier is adjusted to be 39.8 dB from 1.24 Hz to 9.1 KHz. In this bandwidth, the input-referred noise is 33.7 $nV/\sqrt{Hz}$ and the RMS noise is 1.9 μVrms. This novel amplifier can have potential application in the field of neural signal recording and other related fields.

INDEX TERMS Amplifier, MTJ, neural signal, pseudo resistor.

I. INTRODUCTION

Brain-machine interface (BMI) creates one great influence on the biological controlling approach of the human brain. In the BMI system, the neural signals are transmitted from brain to the machine and the data can be stored based on the machine's pattern. The BMI systems have been fully utilized in some academic fields [1]–[3], such as the neuro graphy, the prosthetic movement, the blind glasses, *etc*.

The schematic structure, including its related application of the BMI system, is shown in Fig. 1(a). The BMI system usually consists of microelectrodes, low noise amplifier, band-pass filters and other modules for the signal processing. Among them, the microelectrodes are used to extract neural signals of brain, either in an invasive or non-invasive way. The low noise amplifier is designed effectively to amplify the amplitude of the weak neural signals, which are extracted by the microelectrodes, as shown in Fig. 1(b). The band-pass filter is used to define the frequency channel. The noises and the other interference neural signals can be limited by the filter. Among the key elements of the BMI system, the characteristics of the amplifier have the critical influence on the quality of the neural signals. The neural signals are the electric fields monitored by extracellularly placed electrodes. The potentials caused by the movements of Ca^{2+}, k^{+}, Na^{+}, *etc.* are superimposed to generate the electric potential [4]. So the neural signals extracted on the recording side are the mixed signals including action potentials (spikes), biological noise of surrounding neurons, thermal noise and flick noise of the electrodes [5]. For the neural signals from the brain, some peak information with relative big amplitude is mixed with the other minor information with very small amplitude in the spectrum, in which the noise is also inevitably included. The spectrum of the signals that is produced by the different recording methods is variable with their own specific characteristics. For example, the EEG (electro-encephalo-graphic) is the most widely used way because it does not require invasive surgery. The EEG neural signal can be recorded directly from the scalp by some indirect ways. The collected neural signals are attenuated by the impedance of the skull and other soft tissues [4], [6]. ECoG (electro-cortico-graphy) is recorded from the cortical surface. The spatial resolution

The associate editor coordinating the review of this manuscript and approving it for publication was Cihun-Siyong Gong.

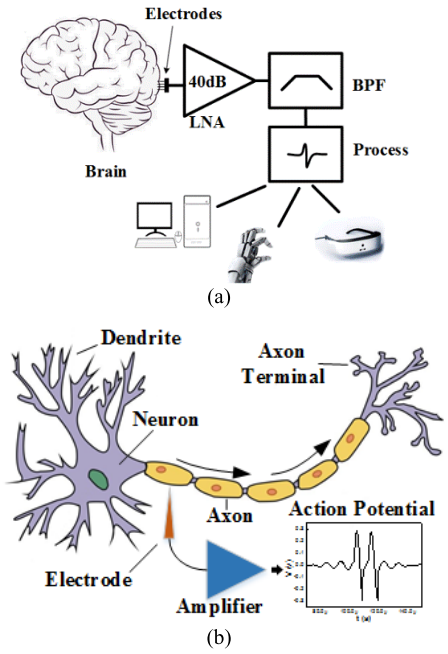

FIGURE 1. (a) The schematic structure and its potential applications of the BMI system. (b) The detailed schematic of the neuron and the amplifier in the BMI system. The information is amplified and filtered by the BMI system.

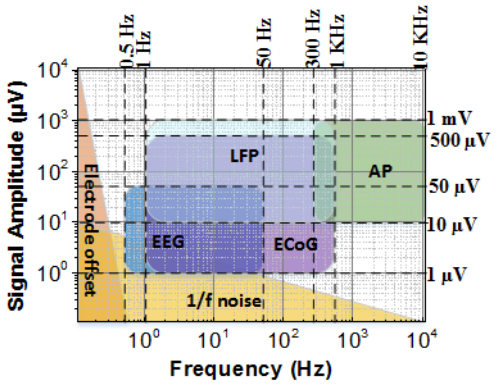

FIGURE 2. The distributions of the amplitude and frequency of EEG, ECoG, LFP, AP, electrode offset, 1/f noise.

and the amplitude of the ECoG signal are better than those of the EEG method. The distance between the recording location and the source [7] is shorter than that of EEG. As the implanted of the microelectrodes in skull, the risk of recording the ECoG is increased. In the LFPs approach, the probes are inserted inside of the brain to extract the neural signal.

The information of the neural signals is extracted and recorded with high bandwidth and high accuracy [4]. Action potentials (spikes) on different neuron have different effects. The information is loaded by the frequency and the pattern in neuronal cells. The spikes are generated by the neurons in certain firing frequency [8]. And the frequency of firing pattern is encoded by the information of neurons [9]. The amplitude of the spikes enhances the spatial resolution of recording [10]. It is transmitted from one neural to the next neural in axons [9]. So the spikes aren't overlapped. The relevant general ranges of the amplitude and frequency are shown in Fig. 2 [11]. With suitable stimulation, the action potentials are generated, with certain frequency and amplitudes. Both of them are considered as the main information [9], [12]. Generally, the amplitude of the spike in the action potential is about 100 μV or even higher [13]. In addition, the frequency and the pattern are various in according to different types of the neurons. For example, the amplitude of the somatic action potentials recorded from layer 5 pyramidal neurons in brain of rats is greater than 80 mV with the width of 20 ms [14]. Spikes recorded by the Neurogrid on the surface of the neocortex and hippocampus were displayed with different frequencies and widths [15].

There is a DC offset of 1-2 V due to the electrochemical effect on the interface between the microelectrode and the related biological tissue, which should be balanced in the system [16]. In addition, the neural signals are highly susceptible to be mixed with other noises, such as the flicker noise with amplitude of 10 μV and the thermal noise with that of 5 μV. Also biological noise mainly arises from the activities of the other hundreds of neurons surrounding the recording microelectrode and relevantly represents accessories as other major source of noise whose level is about 10 μV [5]. So the input reference noise of the amplifier should be lower than the background noise around the recording position [17]. The low spikes include the thermal noise, the flicker noise and the biological noise.

Different structures of the amplifier designed for the BMI system were proposed and demonstrated in previous published works [13], [18]–[22]. Generally, the bio-amplifier design was divided to three categories, including the capacitively-coupled inverting amplifier [18]–[20], the chopper-stabilized amplifier [13], [21] and the amplifier-DAC [22]. The capacitively-coupled amplifier is the most classical ones. In this kind of amplifier, a feedback network comprised by the capacitor and the pseudo resistor is included to reduce the DC offset voltage. To achieve the low-frequency high pass corner and as small area as possible of capacitor, the value of the pseudo resistors should be high enough. For capacitively-coupled amplifier, a feedback network comprised by the capacitor and the pseudo resistor is included to balance the DC offset voltage. The high pass corner of this amplifier is given by $1/2\pi RC$. To make the high pass corner set in as low frequency as possible, the value of the capacitor C or the resistance R should be high enough. However, the high value of capacitor means that the area of capacitor in integrated circuit will be increased to occupy the main area of the chip. The pseudo resistor can provide high resistance by MOSFET with small area. Therefore, as used the pseudo resistor, the small area of capacitor can be used in the amplifier. Many types of pseudo resistor were proposed, such as mos-bio [18] and bias MOSFET (Metal-Oxide-Semiconductor Field Effect Transistor) [23]–[26].

However, the biased MOSFET need the extra bias circuits, which increase the power dissipation of the chip. Because the current following through the MOSFET is asymmetric, the output signals are distorted. To get symmetric current, two matched MOSFETS are always needed to balance the distortion of the output signals. However, the power dissipation on the two MOSFETS is increased dramatically.

The chopper amplifier used in neural signal can remove the flicker noise and the offset voltage by the method of the modulation and de-modulation [13], [21]. The drawback of the chopper amplifier is that the operation bandwidth is limited by the chopper frequency. So, the high frequency action potentials cannot be operated by the chopper amplifier.

The other amplifier is a single differential pair combined with Analog-Digital Converter (ADC) and Digital-Analog Converter (DAC) to set up the mixed-signal feedback for filtering and offset suppression [22]. Modulated by the DAC, the differential pair with transistors of programmable widths biased in sub-threshold region can delete the offset down to sub-1 mV level while reduce the noise caused by current devices. The ADC is used to sample the spike signals separated from the neural signals. This amplifier improved signal-to-noise ratio by multiple feedbacks, though the date of SNR is not mentioned. However, the processing based on the ADC-DAC architecture is time-consuming. So, the approach hasn't been implemented in the BMI system until now.

For the above-mentioned amplifiers, obvious problems exist that interfere in the field of the BMI system. For example, in the previous cases, the operating frequency of the amplifier is designed to match the range of LFPs (up to 200 Hz or 300 Hz). The bandwidth of the action potentials is 300 Hz to 5 KHz [13], [22]. Thereby, the bandwidth of amplifier is modulated to high-pass the spikes and remove the LFPs. However, the frequencies of some action potentials are still included in the range of LFPs. In the reference [27], the width of the action potential in the soma of dentate gyrus granule neurons is 710 ms and its amplitude is about 100 mV. It's difficult to filter the LFPs while hold the spikes if only the frequency is considered during the processing.

To achieve the signal processing requirements of the BMI system, a novel amplifier based on the Spin-Transfer-Torque Magnetic Tunnel Junction (STT-MTJ) device is designed and fulfilled, with the benefit of suppressing the DC offset and getting rid of the unnecessary noise signals while amplifying the action potentials according to different amplitudes and frequencies.

In this paper, a novel bio-amplifier is proposed by integrating the MTJ devices, showing improvements on the performance, including high resistance, selective gain and low noise. Because of the tunnel magnetoresistance (TMR), the amplifier with the MTJ as output impedance exhibits the lower gain for weak signal while shows higher gain for the signal with higher amplitude. As used as the pseudo resistor, the MTJ device doesn't occupy the area of the integrated circuit since it is generally fabricated on the 4^{th} or 5^{th} metal layer. Its resistance can maintain high value and it can minimize the similar non-magnetic 1/f (flicker) noise. Its noise power could be minimized since the current is limited by the high resistance. Because the defects in the MTJ device that are responsible for the resistance fluctuations are getting less and less activated at lower biasing currents, its pseudo resistance shows more promising characteristic than that of MOS device.

The paper is organized as following: Section II describes the schematic and the structure of the amplifier by integrating a pseudo resistor with STT-MTJ device. Its operating mechanism is included in the section. Section III and IV report the results and noise analysis of the pseudo resistor and the novel amplifier proposed in this work. The conclusion is made in the last section.

II. DESIGN OF THE AMPLIFIER

A. DESIGN OF THE MTJ

The asymmetry of spin up electrons and spin down electrons in the two ferromagnetic layers results in the magnetoresistance effect of MTJ. MTJ shows low noise when compared with the diodes [28]. The MTJ device was prepared by using a magnetron sputtering system and patterned with photolithography. The device was then etched using an Argon ion milling process and electrodes were deposited using an electron beam evaporation process. The complete structure was Ta 2nm/(Al 10nm/Cu 3nm)(5)/Al 5nm/Ta 3nm/PtMn 10nm/CoFe 2.5nm/Ru 0.8nm/CoFeB 3nm/ MgO 1.5nm/ CoFeB 3nm/ Ru 3nm/Ta 10nm/Ru 7nm and the size of the fabricated devices was 2 μm x 6 μm. The magnetic properties were measured in a physical properties measurement system (PPMS) using a standard four-probe technique with a sensing current of 0.05 mA. The MTJ consists of two ferromagnetic layers and an oxide barrier layer (also called tunnel barrier layer). Fig. 3(a) shows the structure of the STT-based MTJ, including pinned layer (CoFeB/Ru/CoFe), pinning layer (PtMn), free layer (CoFeB) and the barrier layer (MgO). As shown in Fig. 3(b), the STT-MTJ changes its state according to the direction of the current. I_P is the critical current when the MTJ state is changed from Parallel (P) to Antiparallel (AP). I_{AP} is the critical current when the MTJ state is changed from Antiparallel (AP) to Parallel (P). The MTJ's state will be changed alternatively and show different resistance when the current is beyond the critical value. The fitting curve in Fig. 3(c) shows the MTJ resistances of parallel state (R_P) and antiparallel state (R_{AP}). The low resistance of the MTJ is 200 KΩ while the high resistance is 1000 KΩ. The critical current I_P for R_P-R_{AP} is 5.25 nA, and the critical current I_{AP} for R_{AP}-R_P is 2.7 nA.

B. DESIGN OF THE AMPLIFIER WITH THE MTJ

Neural signals, especially action potentials, are the types that referred to as ''signals with Information Concentration at High Amplitudes (ICHA)'', which means that the intensity of the information is higher on the higher side of the amplitude range [10]. For the neural signals, the amplifier should

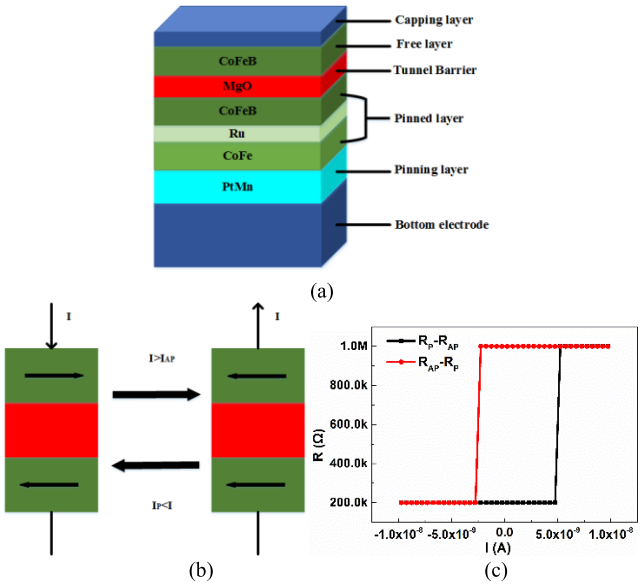

FIGURE 3. The structure of the STT-MTJ. (a) The STT-MTJ is composed of three main layers: a tunnel barrier layer, such as MgO; a pinned layer and a pinning layer consisting of CoFeB, Ru, CoFe, PtMn; a free layer consisiting of CoFeB. Capping layer and bottom electrode are the metal electrode. (b) The STT-MTJ state changes from parallel to anti-parallel if the positive current $|\mathbf{I}| > |\mathbf{I_P}|$, on the contrast, its state will return if negetive current $|\mathbf{I}| > |\mathbf{I_{AP}}|$. (c) The relationship between the resistance and the current, showing the critical currents of $\mathbf{I_P}$ and $\mathbf{I_{AP}}$, respectively.

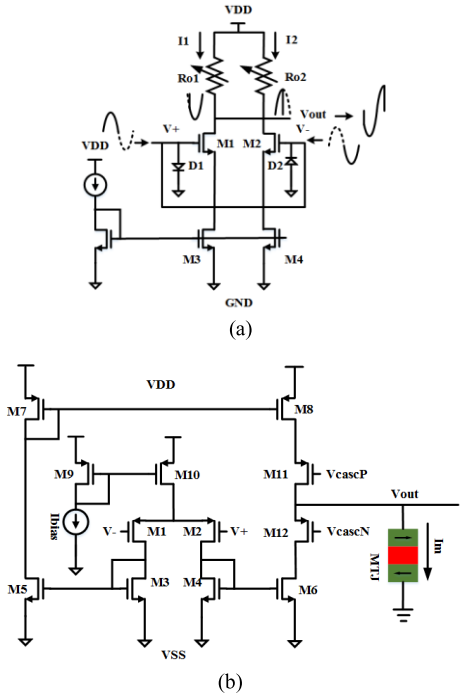

FIGURE 4. (a) Schematic diagram of classical amplifier. (b) The structure of the amplifier.

increase the high amplitudes and suppress the low amplitudes simultaneously. Fig. 4(a) is the schematic diagram of classical amplifier. The circuit is composed by two coincident common source amplifiers. One amplifier includes M1, M3, variable resistor R_{O1}. The other amplifier includes M2, M4, variable resistor R_{O2}. Due to the rectifying effect of the diode D_1, the lower half period of the input signal can be amplified by M1. The threshold voltage of R_{O1} is set to be certain value. If the resistance of R_{O1} increase abruptly when the input signal reaches the threshold voltage, the gain of the amplifier will be increased, following the equation, $A_V = -G_m \times R_{out}$.

Similarly, the diode D_2 rectifies the other half period. M2 is used to amplify the signal. Another negative threshold voltage is set on a certain value. If the resistance of R_{O2} decrease sharply when the input signal down to the threshold voltage, the gain of the amplifier will be decreased accordingly. Based on the above discussion, the peaks with high amplitude can make the amplifier increase the gain at the beginning and return the low gain at the end of the whole cycle. The strength of the signals is varied with the changing of the distance from the recording site to single source. If only the weak signals received, the initial resistance of R_{O1} or R_{O2} is low. So the weak signals will be rejected as lower gain of the amplifier. As a result, the information concentrated on the high amplitudes can be extracted effectively by the amplifier. There is no strict requirement on the absolute values of the two threshold voltages. The absolute values of the two threshold voltages can be set as high as possible, but not higher than the action potentials of the information. In this way, the threshold voltage can be adjusted for different subjects.

In this way, the complementary push-pull output amplifier [18] and a STT-MTJ with variable resistance as the internal structures are proposed in Fig. 4(b). M1 and M2 are two identical PMOS transistors, acting as input differential pairs. The current mirror configuration of M9 and M10 provides bias current of 8 μA for the entire circuit. Through the mirroring of M5 and M7, the output signal of the opposite end of the differential amplifier is transmitted to M8. A cascode structure as the push-pull output stage of the entire amplifier is formed by M6, M8, M11 and M12. The output voltage of the push-pull stage changes around the 0 V potential. Therefore, the current of STT-MTJ also be changed around 0 A. According to the structure in Fig. 4(b), the gain of this structure is estimated by

$$A_v = \frac{V_{out}}{V_{in}} \approx g_{m2}\, g_{m6}\, R_{out1} \left(R_{out2} \,\|R_{MTJ(P,AP)}\right) = g_{m2}\, g_{m6}\, R_{out1} \frac{R_{out2}\, R_{MTJ(P,AP)}}{R_{out2} + R_{MTJ(P,AP)}}, \quad (1)$$

$$R_{out1} \approx r_{o2} \,\|\, r_{o4} \,\|\, 1/g_{m4}\ , \quad (2)$$

$$R_{out2} \approx \{[1 + (g_{m11} + g_{mb11})\, r_{o11}]\, r_{o8}\} \,\|\, [(1 + g_{m6}\, r_{o6})\, r_{o12}], \quad (3)$$

in which R_{out1} and R_{out2} are the output resistance of the first stage and the second stage of the amplifier, respectively. $R_{MTJ(P,AP)}$ is the resistance of MTJ in parallel or anti-parallel state.

The gain of the amplifier is changed by different states of the MTJ controlled by the flowing current. The current of the

MTJ can be expressed as:

$$I_{m(P,AP)} = \frac{V_{out}}{R_{MTJ(P,AP)}} = \frac{V_{in}\, g_{m2}\, g_{m6}\, R_{out1}\left(R_{out2} \,\|\, R_{MTJ(P,AP)}\right)}{R_{MTJ(P,AP)}} \approx V_{in}\, g_{m2}\, g_{m6}\, R_{out1}\, \frac{R_{out2}}{R_{out2} + R_{MTJ(P,AP)}}. \quad (4)$$

The $R_{MTJ(P,AP)}$ is designed to be smaller than the R_{out2}. So the currents of the MTJ depend largely on the input signals V_{in}. The transformation of the MTJ's resistance will occur on two conditions:

1. When the current is flowing reversely;
2. When the current flowing through the MTJ exceeds the critical current.

In the neutral point, the resistance value and amplifier output are still kept on the original state. Because the input signal Vin doesn't exceed the threshold voltage and the current of the MTJ doesn't exceed the critical current. The initial state of the STT-MTJ is set to be the low resistance. The gain will be increased by the high resistance of the STT-MTJ when the Im exceeds the forward direction critical switching current I_P at the positive half cycle. Similarly, the gain decreased by low resistance when the Im exceeds reverse direction critical switching current I_{AP} at the negative half cycle. Thereby, the amplifier exhibits the lower gain for weak signal while shows higher gain for the signal with higher amplitude.

To testify the feasibility of the method proposed above, the structure in Fig. 4(b) is simulated by Hspice software. Figure 5 shows the output voltage (V(vo)) and the current (Im) of the MTJ when the sine signals with the amplitudes of 0.1 mV and 0.07 mV are input. In Fig. 5, i(r) is equal to Im for different resistances and input signals. The current i(r) and output voltage v(o) both fluctuate around the X-axis. For the same resistance, higher input peaks result in high current i(r), such as i(r)/0.07 mV/200 k and i(r)/0.1 mV/200 k. Hence, the critical switching current of the MTJ I_{AP} between this two currents is chosen to make the MTJ operate in the state with high resistance (which means the voltage of the Vout is high by the equation $A_V = -G_m \times R_{out}$) or operate in the state with low resistance (which means the voltage of the Vout is low by the equation $A_V = -G_m \times R_{out}$). When higher input peaks make the output i(r) higher than i(r)/0.07/200 k, the resistance of MTJ will be changed to the anti-parallel state (1000 KΩ). So the gain of amplifier is increased for higher peaks. According to Eqn.4, the critical current for Im is

$$|I_P| = 0.07mV \times g_{m2}\, g_{m6}\, R_{out1}\, \frac{R_{out2}}{R_{out2} + 200K\Omega}, \quad (5)$$

$$|I_{AP}| = 0.1mV \times g_{m2}\, g_{m6}\, R_{out1}\, \frac{R_{out2}}{R_{out2} + 1000K\Omega}. \quad (6)$$

Figure 6 shows the results of this amplifier with different amplitudes of the input signal. The frequency of the input signals is 5 KHz. All the spikes with amplitudes over 0.07 mV are recorded by the amplifier. The initial state of MTJ is "0"

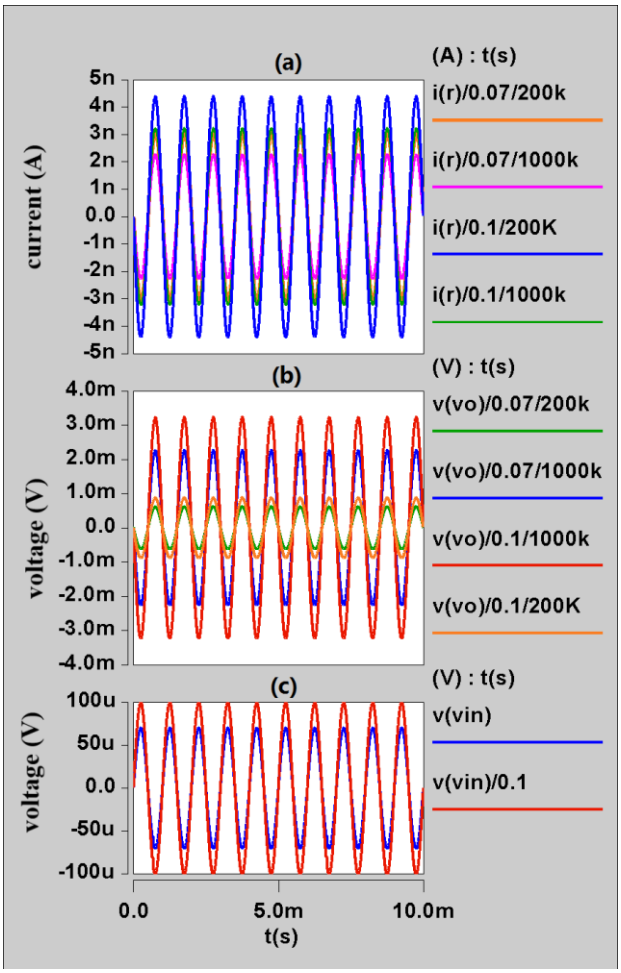

FIGURE 5. The simulation results of the amplifier with STT-MTJ when input the sine signals with the amplitudes of 0. 1 mV and 0.07 mV. (a) The current i(r) at different resistances with the amplitudes of 0.1 mV and 0.07 mV. (b) The output voltage at different resistances with the amplitudes of 0.1 mV and 0.07 mV. (c) The input sine signals with the amplitudes of 0.1 mV and 0.07 mV.

where the resistance of MTJ is 200 KΩ. Because the low amplitude of spikes (such as the noises in neural signals) generate low current of the MTJ at the output of the amplifier, the resistance is low. On this situation, there isn't change on the state. While the state of MTJ keeps "0", the gain of this amplifier is kept low until the positive half current of the MTJ is larger than the critical current I_{AP} due to the high amplitude of spikes (such as the action potentials in neural signals). The resistance of the MTJ is changed into the high state, with resistance up to 1000 KΩ. The state of the MTJ is changed into "1". That make the high spikes can be amplified at a relative high gain since it has slightly higher peaks than others. Following the decrease of the input spikes, the state of the MTJ is changed into "0" accordingly. The gain of amplifier is decreased again. Due to the changing of the MTJ's resistance with the input peaks, the high amplitude peaks are amplified by the designed MTJ-based amplifier. At the same time, the low amplitude peaks are suppressed. The spikes of action potentials are generated by the neurons in certain firing

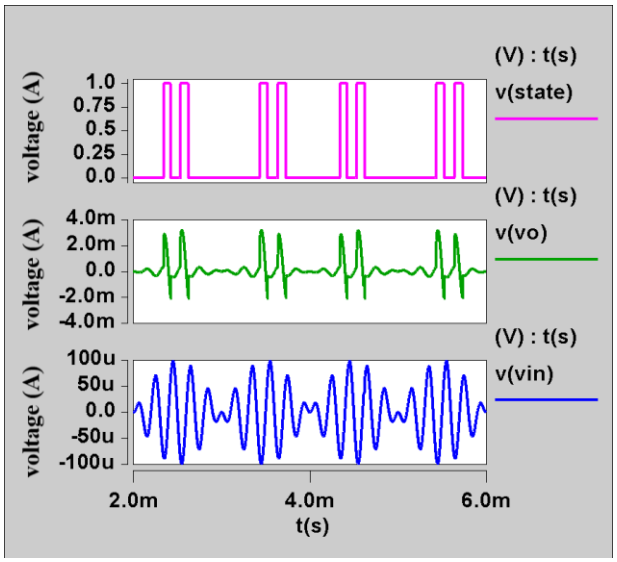

FIGURE 6. The input signals with different amplitudes. The spikes with the amplitude over 70 μV can be recorded by the amplifier.

frequency [8]. And the frequency of firing pattern encodes the information of neurons [9]. The amplitude of spikes enhances the spatial resolution of recording [10]. Even if the spikes will be overlapped with LFPs and noises, the amplitude of action potentials will be increased that will enhance the spatial resolution of recording. So the structure of the amplifier proposed can record the spikes by the way described above.

III. RESULTS AND ANALYSIS OF PSEUDO RESISTOR AND AMPLIFIER

A. THE PERFORMANCE OF PSEUDO RESISTOR

The DC offset generated on the interface between the microelectrode and the related biological tissue disturbs the recognition of the neural signals. Based on the amplifier proposed above, the feedback loops consist of pseudo resistors and capacitors are added to eliminate the DC offset. Figure 7 shows three different types of the pseudo resistors, including single MOS (Fig. 7(a)), MOS+MOS (Fig. 7(b)), and the proposed MOS+MTJ (Fig. 7(c)). The pseudo resistor integrated with the STT-MTJ and MOSFET device is proposed and designed. As shown in Fig. 7(c), the designed pseudo resistor constituted by the MTJ device and a PMOS shows ultra-high resistance. The gate and the source of the PMOS are connected with the drain and the base substrate respectively. To describe the characteristic of the pseudo resistor, the comparison among of the three modes including MTJ+MOS, single MOS and MOS+MOS, are made as shown in Fig. 8.

FIGURE 7. Three different pseudo resistance devices, single MOS, MOS+MOS, MOS+MTJ.

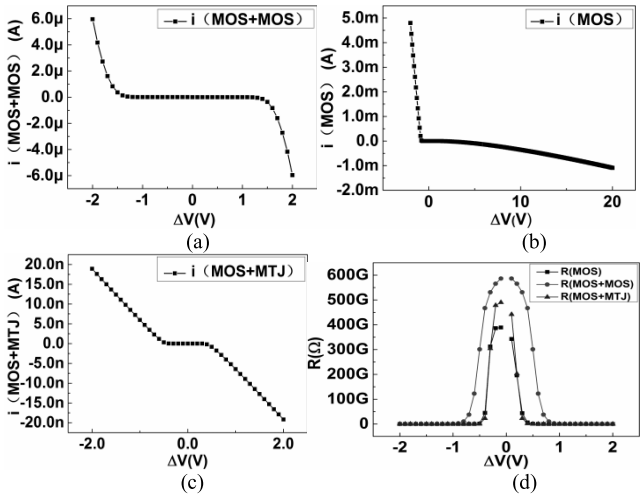

FIGURE 8. The DC characteristics of pseudo resistors, MOS+MOS(a), single MOS(b), MOS+MTJ(c). (d) The V-R of these three pseudo resistors. The resistances of the single MOS, MOS+MOS and MOS+MTJ are high up to 388 GΩ, 583 GΩ, 495 GΩ respectively.

The experimental DC characteristics of three pseudo resistors are shown in Fig. 8(a), (b) and (c), separately. The resistance variable with the voltage, $(V_f - V_o)$, is shown in Fig. 8 (d). Three modes of the resistors all show high resistances to meet the need of the filter net when $(V_f - V_o)$ is low. The single-MOS-mode shows a resistance up to 388 GΩ, while 495 GΩ for MTJ+MOS and 583 GΩ for MOS+MOS. Even if the resistance of MOS+MTJ changes a little when the voltage difference ΔV is less than 100 mV, the resistance still hold an high resistance at 400 GΩ that is high enough to make the high pass corner keep in low frequency. As shown in Fig. 8(b), the current of the single-MOS mode is asymmetric, which leads the distorted output signal due to the offset of the DC characteristics. That is a major factor limiting the dynamic range of the low voltage circuit [23].

B. RESULTS OF THE AMPLIFIER

The amplifier proposed in this paper is shown in Fig. 9. This amplifier is a preamplifier of the whole BMI system to reduce the noise and remove the DC offset. So the very high gain

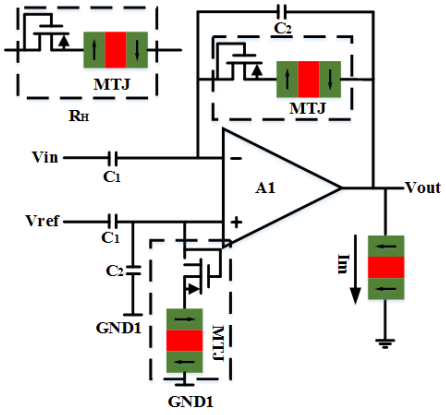

FIGURE 9. Overall schematic of the neural amplifier with STT-MTJ.

is not the urgent need. In general, the gain of the amplifier with 20-40 dB is enough to process the neural signals [29]. The losed-loop gain of the amplifier is C_1/C_2, determined by the input capacitor C_1 and the feedback capacitor C_2. The low cutoff frequency network consists of R_H and the feedback capacitor C_2. The purpose of eliminating the DC offsets is achieved by the high-pass point $F_1 = (2\pi R_H C_2)^{-1}$.

The amplifier is fabricated in the 0.35 μm CMOS process as shown in Fig. 10. The layout of the amplifier is shown in Fig. 10(a). The SEM image of the MTJ device is shown in Fig. 10(b). It shows the layout of the designed amplifier, with STT-MTJ devices deposited on the top metal layer, with the same structure as shown in Fig. 4. The results of the amplifier shown in Fig. 11-14 are measured by signal analyzer. As shown in Fig. 11(a), the amplifier has a gain of 39.8 dB in the mid-band and a phase margin of ab out 50 degrees, which indicates that the amplifier is in a stable state. The power of the amplifier is 36.1 uW. Otherwise, to ensure the reduction of the disturb of other unnecessary signals in low frequency, the bandwidth of the amplifier is also designed from 250 Hz to 9.1 KHz as shown in Fig. 11(b). The bandwidth range is about 9.1 kHz with the low cut-off frequency of 1.24 Hz. The frequency of typical action potentials is high up to 7 KHz [13], [18] or 10 KHz [10], [29].

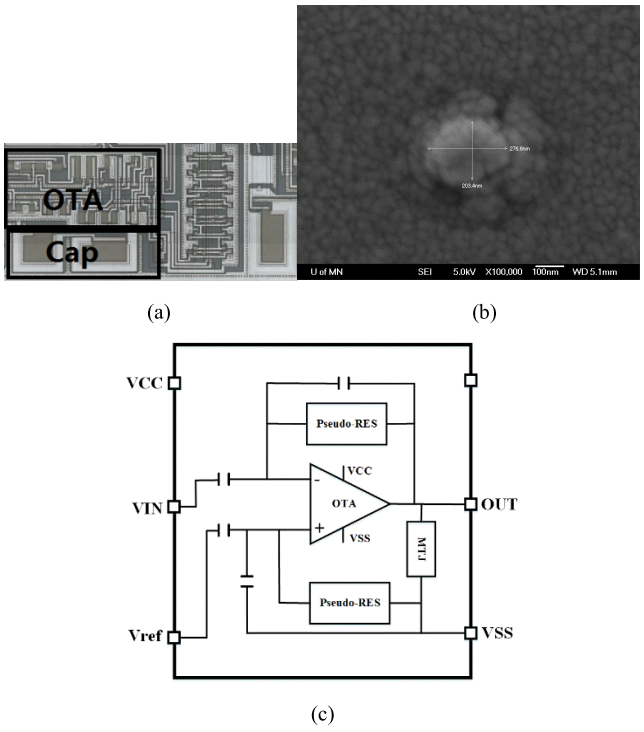

FIGURE 10. The layout of the amplifier. The area of OTA is 0.15 mm × 0.3 mm. (a) The layout of the OTA circuit. (b) The top layer is the MTJ device, with size 276 nm × 200 nm. (c) The diaphragm of Layout with Pin.

Therefore, the bandwidth of this amplifier is suitable for the neural signals. The low cut-off frequency makes the amplifier suppress the DC offset of the doping in the input signal while amplifying the weak biological signal. The gain

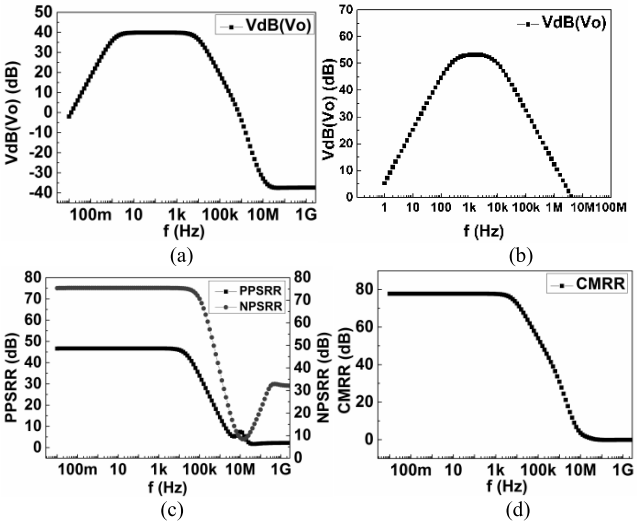

FIGURE 11. (a) The gain of the amplifier is 39.8 dB with the bandwidth from 1.24 Hz to 9.1 KHz. (b) The gain of the redesigned amplifier is 53 dB with the bandwidth from 250 Hz to 9.1 KHz. (c) The PPSRR and NPSRR of the amplifier is 48 dB with the bandwidth of from 250 Hz to 9.1 KHz. (d) The CMRR of the amplifier is 78 dB.

of the common mode is

$$A_{CM} = -\frac{\left(g_{m1}+g_{m2}\right)\left(R_{o3}\,\|R_{o4}\right)}{1+\left(g_{m1}+g_{m2}\right)R_{o10}} \cdot\frac{1}{4}\,g_{m6}\left[\left(g_{m11}+g_{mb11}\right)r_{o12}\right]r_{o8}\,\|\left(1+g_{m6}\,r_{o6}\right)r_{o12} \tag{7}$$

So, the CMRR is

$$\begin{aligned} CMRR &= \frac{A_v}{A_{CM}} \\ &= \frac{g_{m2}\,g_{m6}\,R_{out1}\,\frac{R_{out2}\,R_{MTJ(P,AP)}}{R_{out2}+R_{MTJ(P,AP)}}}{\frac{(g_{m1}+g_{m2})(R_{o3}\|R_{o4})}{1+(g_{m1}+g_{m2})R_{o10}}\cdot\frac{1}{4}\,g_{m6}[(g_{m11}+g_{mb11})r_{o12}]r_{o8}\,\|(1+g_{m6}\,r_{o6})r_{o12}} \\ &= \frac{4g_{m2}\,R_{out1}\,R_{o10}\,\frac{R_{out2}\,R_{MTJ\,(P,AP)}}{R_{out2}+R_{MTJ\,(P,AP)}}}{\left(R_{o3}\,\|R_{o4}\right)\cdot\left(g_{m11}\,r_{o12}\,r_{o8}\,\|g_{m6}\,r_{o6}\,r_{o12}\right)} \end{aligned} \tag{8}$$

The PSRR is calculated by

$$PSRR = \frac{A_v}{A_{DD}} = \frac{g_{m2}\,g_{m6}\,R_{out1}\,\frac{R_{out2}\,R_{MTJ\,(P,AP)}}{R_{out2}+R_{MTJ\,(P,AP)}}}{g_{m10}\,r_{o10}\left(\left(\left(r_{o2}+r_{o4}\right)/g_{m2}\,r_{o2}\right)\|r_{o10}\right)} \tag{9}$$

Fig. 11(c) and (d) show the positive PSRR (48 dB), negative PSRR (75 dB) and the CMRR (78 dB) of the amplifier.

Figure. 12 shows the input neural signal spectrum of rat on electrodes, including high and low amplitudes, LFPs with wide frequency ranges and other noises from surrounding neurons and circuits. Due to the disturbance of the LFPs and the other noises, it is a challenge to recognize the action potential precisely. For the convenience of the processing of the signals, the necessary action potentials should be extracted and amplified while the other signals should be

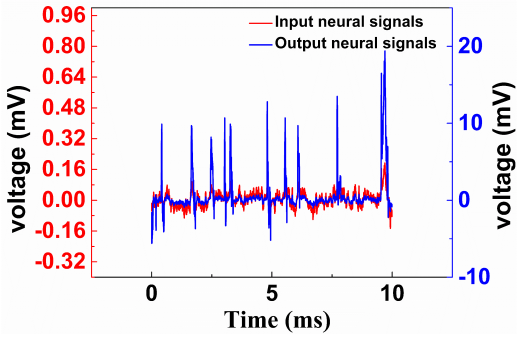

FIGURE 12. Red line: The input neural signals recorded from the stimulated rat. Blue line: The processed neural signals, including obvious action potentials while the other information is suppressed.

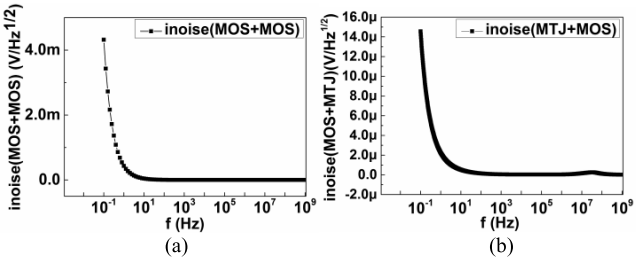

FIGURE 13. (a) The input-referred noise of the amplifier with the MOS+MOS is 126.7 nV/$\sqrt{\text{Hz}}$, the RMS noise is 33 μVrms at the frequency from 1.04 Hz to 5.6 KHz. (b) The input-referred noise of the amplifier with the MTJ+MOS is 33.7 nV/$\sqrt{\text{Hz}}$, the RMS noise is 1.9 μVrms at the frequency from 1.24 Hz to 10 KHz.

suppressed. The blue line in Fig. 12 shows the action potentials extracted from the interferential signals by the suitable processing of the signals. The processed signal (blue line) shows clear pattern and amplitude by comparison with the input extracted data (red line). On this sense, a suitable amplifier with the functions of amplifying and processing is highly required for the BMI system.

C. THE ANALYSIS OF NOISE

Even if the resistance of MOS+MOS pseudo resistor is higher than that of MOS+MTJ, the MTJ device can help to optimize the noise characteristics. The MTJ shows potential merits in noise reduction and the area saving in the amplifier. The pseudo resistor of RC feedback network should hold as possible as high resistance so that the area of capacitor can be decreased. The resistance of MTJ is inversely proportional to the area [30]. Therefore, the MTJ can show high resistance while occupy small area.

The noise of the amplifer is given by

$$v_{ni,thermal}^2 = \left[\frac{16kT}{3g_{m1}}\left(1 + 2\frac{g_{m3}}{g_{m1}} + \frac{g_{m7}}{g_{m1}}\right)\right]f. \qquad (10)$$

To lower the noise of the amplifier, g_{m3} and g_{m7} should be smaller than g_{m1}. So $(W/L)_3$ and $(W/L)_7$ should be decreased as much as possible [18]. The flicker noise in PMOS of the input differential pair is one or two oders of magnitude lower than the flicker noise in NMOS.

The noise spectrum of the MTJ can be described by the Eqn.11:

$$S_v = 2eVR\coth\left(\frac{eV}{2k_BT}\right) + \frac{\alpha V^2}{Af^\gamma} \qquad (11)$$

where V is the bias voltage. R is the resistance of the MTJ. e is the electron charge. k_B is the Boltzmann constant. T is the temperature. A is area of the junction, f is the frequency γ is the exponent and α is the Hooge-like parameter.

In Eqn. 11 the first term represents the thermal noise and the shot noise. The second term represents the flicker noise. Based on Eqn. 11, the noise of the MTJ is increased when the area is decreased. However, the high frequency of neural signal (high up to ~KHz) weakens the area's influence on the noise. In fact, shrinking the MTJ area is an effective way to minimize the similar non-magnetic 1/f noise [31], [32]. The coth(eV/2k_BT) term in Eqn. 8 can be ignored when the voltage V is less than 150 mV. Generally, the most output signals of the amplifier is below 100 mV. So the shot noise of the MTJ is too small to be considered. The small area and the weak bias voltage contribute to the weak current of the MTJ.

The high resistance of the MTJ device increases the noise. However, the noise power spectra of the MTJ under different bias currents indicates the decrement of the noise power with decreasing bias current [33]. The current of the MTJ is as low as a few picoamperes because of its high resistance. So the low current of the MTJ decrease the noise power. Figure 13 shows the noise results. It is demonstrated that the flicker noise of the amplifier with MOS+MTJ is lower than that of the amplifier of MOS+MOS pseudo-resistor.

The input-referred noise of the amplifier with the MTJ+MOS pseudo resistor shown in Fig. 13(b) is 33.7 nV$\Big/\sqrt{\text{Hz}}$. The RMS noise is 1.9 μVrms at the frequency from 1.24 Hz to 10 KHz, which is lower than that of the amplifier of MOS+MOS pseudo-resistor shown in Fig. 13(a). It can be seen that the flicker noise at low frequency is the main part of the noise. The high flicker noise below 1.24 Hz is removed. The noise efficiency factor (NEF) is used to express the degree of influence of noise in the amplifier. NEF is used to evaluate the efficiency of the bias current of the amplifier for noise [34]. The equation is as shown in Eqn. 12:

$$NEF = V_{ni,rms}\sqrt{\frac{I_{total}}{4kT\cdot V_T\cdot\pi/2\cdot BW}}. \qquad (12)$$

where k is the Boltzmann constant (approximately 1.38×10^{-23} $m^2kgs^{-2}K^{-1}$). T is the temperature (human body temperature 310 K). V_T is the thermal voltage (26.7 mV at body temperature). I_{total} is the total current flowing through the amplifier. BW is the amplifier's −3 dB bandwidth. And $V_{ni,rms}$ is the input RMS noise of the amplifier. By the result of this amplifier, the NEF is about 2.9. The input referred noise is the lowest in the manuscript. However, the total current is high. So the NEF is higher than those of the Harrison's and Woradon's works. The Fig. 14(a) shows

TABLE 1. Performance comparison between this work and other recently published works s.

Parameter	Harrison (2003)	Woradorn (2007)	Qinwei Fan (2011)	Rikky Muller (2012)	Tan Yang (2015)	Yin Zhou (2015)	Hariprasad (2017)	This work
Supply voltage(V)	±2.5	2.8	1	0.5	1	1	1.2	±2.5
Supply current(μA)	16	2.7	2.1	-	2.85	3.6	-	16
Gain (dB)	40	40.85	40	-	58.7	40	25.7	39.8
Bandwith (Hz)	0.13-7.5 K	45-5.32 K	0.5-100	300-10 K	49-10.5 K	0.5-10 K	0.12-5 K	1.24-9.1 K
Low-frequency cutoff (Hz)	0.13	45	0.5	300	49	0.5	0.12	1.24
Input noise ($nV\sqrt{Hz}$)	21	31	60	-	-	60	-	33.7
Input-reffered noise(μ Vrms)	2.4	3.06	1	4.9	3.04	-	5.3	1.9
NEF	2.1	2.67	6.7	5.99	3.04	-	4.4	2.9
CMRR (dB)	⩾42	66	134	75	68	96	78	78
PSRR (dB)	⩾42	75	120	64	65	-	76	48/75
Technology	1.5um CMOS	0.5 um CMOS	65nm CMOS	65 nm CMOS	90 nm CMOS	0.18 um CMOS	40 nm CMOS	0.35um CMOS

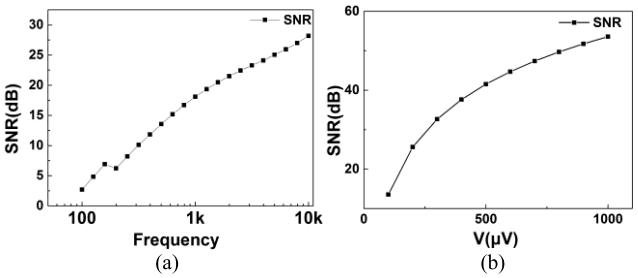

FIGURE 14. (a) The variation of SNR with frequency. The sine signals with frequency from 300 Hz to 5 KHz, 100 μV amplitude and 20 ms duration is inputted to get the SNR. (b) The variation of SNR of amplitudes. The sine signals with 5 KHz frequency, amplitudes from 100 μV to 1 mV and 20 ms duration is inputted to get the SNR.

the variation of SNR with frequency. The sine signals with frequency from 300 Hz to 5 KHz, 100 μV amplitude and 20 ms duration are inputted to get the SNR. The Fig. 14(b) shows the variation of SNR of amplitudes. The sine signals with 5 KHz frequency, amplitudes from 100 μV to 1 mV and 20 ms duration are inputted to get the SNR. The comparison among this work and others [17], [18], [21], [26], [35] is summarized in Table. 1.

IV. CONCLUSION

A low noise amplifier specific for the neural signals. Based on the STT-MTJ spintronic devices is proposed and demonstrated in the paper. The amplifier selectively amplifies the high amplitude peaks, while suppresses the low amplitude peaks. In this way, the novel amplifier can be used to amplify the useful neural signals not only based on the frequency but also on the amplitude.

For suppressing DC offset with the capacitor, a pseudo-resistive device composed of MTJ and MOSFET is proposed in the paper. Compared with the single MOS and the MOS+MOS, it shows better characterizations. Since the resistance of MTJ is changed with the different current flowing directions, the output resistance of the complementary push-pull amplifier can be changed accordingly. So its gain can be tuned according to the input signals. This amplifier achieves gain of 39.8 dB in a bandwidth between 1.24 Hz and 9.1 kHz with the input reference noise of 1.9 μVrms and the noise efficiency factor NEF of 2.9. For the action potentials generated in the same frequency range of LFPs, the proposed amplifier can be effectively amplify the high peaks signals and remove the disturbance of the other noises from the surrounding neural signals.

REFERENCES

[1] X. Fan, L. Bi, and Z. Wang, "Detecting emergency situations by monitoring drivers' states from EEG," presented at the ICME Int. Conf. Complex Med. Eng. (CME), Kobe, Japan, Jul. 2012.

[2] J. Bai, S. Lian, Z. Liu, K. Wang, and D. Liu, "Smart guiding glasses for visually impaired people in indoor environment," *IEEE Trans. Consum. Electron.*, vol. 63, no. 3, pp. 258–266, Aug. 2017.

[3] A. R. Murguialday, V. Aggarwal, A. Chatterjee, Y. Cho, R. Rasmussen, B. O'Rourke, S. Acharya, and N. V. Thakor, "Brain-computer interface for a prosthetic hand using local machine control and haptic feedback," presented at the IEEE 10th Int. Conf. Rehabil. Robot., Noordwijk, The Netherlands, Jun. 2007.

[4] G. Buzsáki, C. A. Anastassiou, and C. Koch, "The origin of extracellular fields and currents—EEG, ECoG, LFP and spikes," *Nature Rev. Neurosci.*, vol. 13, no. 6, pp. 407–420, May 2012.

[5] S. F. Lempka, M. D. Johnson, M. A. Moffitt, K. J. Otto, D. R. Kipke, and C. C. McIntyre, "Theoretical analysis of intracortical microelectrode recordings," *J. Neural Eng.*, vol. 8, no. 4, Aug. 2011, Art. no. 045006.

[6] M. X. Cohen, "Where does EEG come from and what does it mean?" *Trends Neurosci.*, vol. 40, no. 4, pp. 208–218, Apr. 2017.

[7] G. Schalk, "Can electrocorticography (ECoG) support robust and powerful brain–computer interfaces?" *Front Neuroeng.*, vol. 3, p. 9, Jun. 2010.
[8] E. W. Schomburg, C. A. Anastassiou, G. Buzsaki, and C. Koch, "The spiking component of oscillatory extracellular potentials in the rat hippocampus," *J. Neurosci.*, vol. 32, no. 34, pp. 11798–11811, Aug. 2012.
[9] B. P. Bean, "The action potential in mammalian central neurons," *Nature Rev. Neurosci.*, vol. 8, no. 6, pp. 451–465, Jun. 2007.
[10] M. Judy, A. M. Sodagar, R. Lotfi, and M. Sawan, "Nonlinear signal-specific ADC for efficient neural recording in brain-machine interfaces," *IEEE Trans. Biomed. Circuits Syst.*, vol. 8, no. 3, pp. 371–381, Jun. 2014.
[11] R. Muller, H.-P. Le, W. Li, P. Ledochowitsch, S. Gambini, T. Bjorninen, A. Koralek, J. M. Carmena, M. M. Maharbiz, E. Alon, and J. M. Rabaey, "A minimally invasive 64-channel wireless μECoG implant," *IEEE J. Solid-State Circuits*, vol. 50, no. 1, pp. 344–359, Jan. 2015.
[12] L. G. Nowak, R. Azouz, M. V. Sanchez-Vives, C. M. Gray, and D. A. McCormick, "Electrophysiological classes of cat primary visual cortical neurons *in vivo* as revealed by quantitative analyses," *J. Neurophysiol.*, vol. 89, no. 3, pp. 1541–1566, Mar. 2003.
[13] H. Chandrakumar and D. Marković, "An 80-mVpp linear-input range, 1.6-GΩ input impedance, low-power chopper amplifier for closed-loop neural recording that is tolerant to 650-mVpp common-mode interference," *IEEE J. Solid-State Circuits*, vol. 52, no. 11, pp. 1–18, Nov. 2017.
[14] G. Stuart, J. Schiller, and B. Sakmann, "Action potential initiation and propagation in rat neocortical pyramidal neurons," *J. Physiol.*, vol. 505, no. 3, pp. 617–632, Dec. 1997.
[15] D. Khodagholy, "NeuroGrid: Recording action potentials from the surface of the brain," *Nature Neurosci.*, vol. 18, no. 2, pp. 310–315, Feb. 2015.
[16] K. D. Wise and J. B. Angell, "A low-capacitance multielectrode probe for use in extracellular neurophysiology," *IEEE Trans. Biomed. Eng.*, vol. BME-22, no. 3, pp. 212–219, May 1975.
[17] W. Wattanapanitch, M. Fee, and R. Sarpeshkar, "An energy-efficient micropower neural recording amplifier," *IEEE Trans. Biomed. Circuits Syst.*, vol. 1, no. 2, pp. 136–147, Jun. 2007.
[18] R. R. Harrison and C. Charles, "A low-power, low-noise CMOS amplifier for neural recording applications," *IEEE J. Solid-State Circuits*, vol. 38, no. 6, pp. 958–965, Jun. 2003.
[19] F. Corradi and G. Indiveri, "A neuromorphic event-based neural recording system for smart brain-machine-interfaces," *IEEE Trans. Biomed. Circuits Syst.*, vol. 9, no. 5, pp. 699–709, Oct. 2015.
[20] F. Zhang, J. Holleman, and B. P. Otis, "Design of ultra-low power biopotential amplifiers for biosignal acquisition applications," *IEEE Trans. Biomed. Circuits Syst.*, vol. 6, no. 4, pp. 344–355, Aug. 2012.
[21] Q. Fan, F. Sebastiano, J. H. Huijsing, and K. A. A. Makinwa, "A 1.8 μW 60 nV/$\sqrt{}$Hz capacitively-coupled chopper instrumentation amplifier in 65 nm CMOS for wireless sensor nodes," *IEEE J. Solid-State Circuits*, vol. 46, no. 7, pp. 1534–1543, Jul. 2011.
[22] R. Müller, S. Gambini, and J. M. Rabaey, "A 0.013 mm^2, 5μW, DC-coupled neural signal acquisition IC with 0.5 V supply," *IEEE J. Solid-State Circuits*, vol. 47, no. 1, pp. 232–243, Jan. 2012.
[23] X. Zou, X. Xu, L. Yao, and Y. Lian, "A 1-V 450-nW fully integrated programmable biomedical sensor interface chip," *IEEE J. Solid-State Circuits*, vol. 44, no. 4, pp. 1067–1077, Apr. 2009.
[24] D. Han, Y. Zheng, R. Rajkumar, G. S. Dawe, and M. Je, "A 0.45 V 100-channel neural-recording IC with sub-μW/channel consumption in 0.18 μm CMOS," *IEEE Trans. Biomed. Circuits Syst.*, vol. 7, no. 6, pp. 735–746, Dec. 2013.
[25] M. S. Chae, Z. Yang, M. R. Yuce, L. Hoang, and W. Liu, "A 128-channel 6 mW wireless neural recording IC with on-the-fly spike sorting and UWB transmitter," presented at the IEEE Int. Solid-State Circuits Conf.-Dig. Tech. Papers, San Francisco, CA, USA, Feb. 2008.
[26] T. Yang and J. Holleman, "An ultralow-power low-noise CMOS biopotential amplifier for neural recording," *IEEE Trans. Circuits Syst. II, Exp. Briefs*, vol. 62, no. 10, pp. 927–931, Oct. 2015.
[27] J. R. P. Geiger and P. Jonas, "Dynamic control of presynaptic Ca^{2+} inflow by fast-inactivating K^+ channels in hippocampal mossy fiber boutons," *Neuron*, vol. 28, no. 3, pp. 927–939, Dec. 2000.
[28] F. A. Cardoso, R. Ferreira, S. Cardoso, J. P. Conde, V. Chu, P. P. Freitas, J. Germano, T. Almeida, L. Sousa, and M. S. Piedade, "Noise characteristics and particle detection limits in diode+MTJ matrix elements for biochip applications," *IEEE Trans. Magn.*, vol. 43, no. 6, pp. 2403–2405, Jun. 2007.
[29] D. J. Yeager, "Wireless neural interface design," Eng. Elect. Eng. Comput. Sci., Univ. California, Berkeley, Berkeley, CA, USA, Tech. Rep. UCB/EECS-2014-218, 2014.
[30] Y. C. Lee, C. T. Chao, L. C. Li, Y. W. Suen, L. Horng, T.-H. Wu, C. R. Chang, and J. C. Wu, "Magnetic tunnel junction based out-of-plane field sensor with perpendicular magnetic anisotropy in reference layer," *J. Appl. Phys.*, vol. 117, no. 17, Mar. 2015, Art. no. 17A320.
[31] C. Zheng, X. Li, R. D. Shull, P. J. Chen, and P. W. T. Pong, "Comprehensive noise characterisation of magnetic tunnel junction sensors for optimising sensor performance and temperature detection," *Mater. Res. Innov.*, vol. 19, pp. S53–S57, May 2015.
[32] R. Guerrero, F. G. Aliev, R. Villar, J. Hauch, M. Fraune, and G. Güntherodt, "Low-frequency noise and tunneling magnetoresistance in Fe(110)/MgO(111)/Fe(110) epitaxial magnetic tunnel junctions," *Appl. Phys. Lett.*, vol. 87, no. 4, Jun. 2005, Art. no. 042501.
[33] B. Das, Y. C. Lee, L. C. Li, L. Yi-Shiou, Y. W. Suen, L. Horng, T.-H. Wu, C. R. Chang, and J.-C. Wu, "Low-frequency noise characterization of CoFeB/MgO/CoFeB MTJ-based perpendicular field sensor," *IEEE Trans. Magn.*, vol. 52, no. 7, Jul. 2016, Art. no. 4001004.
[34] M. S. J. Steyaert and W. M. C. Sansen, "A micropower low-noise monolithic instrumentation amplifier for medical purposes," *IEEE J. Solid-State Circuits*, vol. 22, no. 6, pp. 1163–1168, Dec. 1987.
[35] Y. Zhou, X. Wu, P. Sun, and M. Zhao, "A 3.6 μW 60 nV/sqrtHz capacitively-coupled instrumentation amplifier for biopotential signal recordings," *J. Circuits, Syst. Comput.*, vol. 24, no. 6, Jul. 2015, Art. no. 1550089.

GUANGCHEN PAN was born in Shandong, China, in 1994. He received the B.S. degree in microelectronics science and engineering from the North University of China, Shanxi, China, in 2017. He is currently pursuing the M.S. degree in integrated circuit engineering with the Department of Microelectronics, Internet of Things Engineering College, Jiangnan University, Wuxi, China, in 2017, under the Supervision of Prof. Y. Jiang.

ALI KARYMY was born in Tehran, Iran, in March 1968. He received the bachelor's degree in physiotherapy from Tehran Shahid Beheshti University, in 1991, the master's degree in physiology from Tehran Tarbiat Modaress University, in 1995, the bachelor's degree in electrical communication engineering from Tehran Shahre Rey Azad University, in 2001, and the master's degree in bioelectric engineering (biomedica engineering) from the Nanjing University of Aeronautic and astronautic (NUAA), in 2013. He is currently pursuing the Ph.D. degree in control science and engineering with Jiangnan University, Wuxi, China. His interest includes computer human body interface.

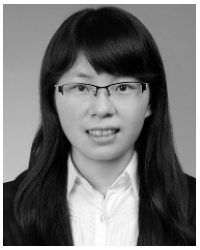

PINGPING YU received the P.D. degree in materials process engineering from Donghua University, in 2014. Since then, she was a Postdoctoral Fellow with the Department of Materials Science, Fudan University, China. She is currently a Lecturer with the Department of Electronic Engineering, Jiangnan University, Wuxi, China. Her current research interest includes the fabrication and application of organic/inorganic semiconductor-based supercapacitors and photodetectors.

YANFENG JIANG was born in Jilin, China, in August 1972. He received the B.S. degree in electrical engineering from Southeast University, in 1993, and the Ph.D. degree in microelectronics from Lanzhou University, in 2000. He is currently a Full Professor with Jiangnan University, Wuxi, China. His research interests include integrated circuit design, power semiconductor devices, and magnetic devices.